Available online at www.sciencedirect.com
SCIENCE DIRECT
Astroparticle Physics 25 (2006) 47–56
Astroparticle Physics
www.elsevier.com/locate/astropart

UHE neutrino damping in a thermal gas of relic neutrinos

J.C. D'Olivo, L. Nellen, S. Sahu, V. Van Elewyck *

Instituto de Ciencias Nucleares, Universidad Nacional Autónoma de México, Circuito Exterior S/N, C.U., 04510 México D.F., Mexico

Received 24 September 2005; received in revised form 30 October 2005; accepted 23 November 2005
Available online 27 December 2005

Abstract

We present a calculation of the damping of an ultra-energetic cosmic neutrino (UHEν) travelling through the thermal gas of relic neutrinos, using the formalism of finite-temperature field theory. From the self-energy diagram due to Z exchange, we obtain the annihilation cross-section for an UHEν interacting with an antineutrino from the background. This method allows us to derive the full expression for the UHEν transmission probability, taking into account the momentum of relic neutrinos. We discuss the effect of thermal motion on the shape of the absorption dips for different UHEν fluxes as well as in the context of relic neutrino clustering. We find that for ratios of the neutrino mass to the relic background temperature 10^2 or smaller, the thermal broadening of the absorption lines could significantly affect the determination of the neutrino mass and of the characteristics of the population of UHEν sources.
© 2005 Elsevier B.V. All rights reserved.

Keywords: Finite-temperature field theory; Neutrino–neutrino interactions; Relic neutrinos; Neutrino mass; Ultra-high energy neutrino fluxes; Absorption lines

1. Introduction

One of the predictions of Big Bang Cosmology is that the Universe is filled with a background of neutrinos, analogous to the cosmic microwave background, but with a lower temperature $T_{\nu 0} \approx 1.95\,\mathrm{K}$ $(1.69 \times 10^{-4}\,\mathrm{eV})$ and a number density $n_{\nu 0} \approx 56\,\mathrm{cm}^{-3}$ per species [1,2]. The direct detection of this cosmological relic background is extremely difficult because of the very small interaction cross-section of low energy neutrinos. It is therefore interesting to explore the possibility of probing the cosmic neutrino background (CνB) with ultra-high energy neutrinos (UHEν). At high energies, the Z resonance in the s channel for the process $\nu\bar{\nu} \to X$ enhances the probability for the interaction of an UHEν with the CνB [3–8]). This process has also been proposed as a possible mechanism for generating UHE cosmic rays through the hadronic decay of the Z boson ("Z-burst" mechanism [9–13]). In that context, it has been pointed out that some features of the CνB (in particular the relic neutrino masses, energy spectra and densities) might be indirectly inferred from the observed spectrum of UHE cosmic rays [14,15]. On the other hand, the resonant production of Z through $\nu\bar{\nu}$ annihilation also results in absorption dips in the UHEν spectrum. If these absorption lines can be observed at Earth with the appropriated resolution, their study would lead us more directly to the same goal: to perform relic neutrino spectroscopy, thereby providing us with evidence for the existence of the CνB and with an independent way of determining the absolute neutrino mass (for recent discussions on the subject, see [16,17]).

Most of the work in the literature assumes that the relic neutrinos are at rest. For small neutrino masses, though, the average momentum can be comparable to the neutrino mass. In this paper, we compute the dominant contribution to the interaction of an UHEν with the CνB using finite-temperature field theory (FTFT). This formalism allows us to take effects due to the neutrino background into account in a systematic and elegant way. In Section 2, we evaluate the damping of a UHEν travelling through the

* Corresponding author.
E-mail address: vero@nucleares.unam.mx (V. Van Elewyck).

0927-6505/$ - see front matter © 2005 Elsevier B.V. All rights reserved.
doi:10.1016/j.astropartphys.2005.11.005

CνB in terms of the imaginary part of the neutrino self-energy. From the damping we determine the absorption probability for an UHEν emitted at a given redshift. We then present in Section 3 some illustrations of our calculation in realistic physical contexts. First, the shape and position of the absorption lines in the spectrum of UHEν from interactions with the CνB depend on the mass of the neutrinos and on the type and distribution of sources for UHEν. We explore various combinations of parameters to investigate the differences between the finite-temperature calculation and previous approximations and to determine the regimes in which those approximations break down and thermal effects become significant. Then we further illustrate our results in the context of relic neutrino clustering for different hypothesis on the density and scale of the clusters. Conclusions are drawn in Section 4.

2. Damping rate and transmission probability of an UHEν

2.1. Self-energy in the relic neutrinos thermal background

The dispersion relation of a particle that propagates through a medium is determined from the linear part of the effective field equation. In momentum space, for a neutrino with four-momentum k^μ and mass m_ν, it takes the form

$$(\not{k} - m_\nu - \Sigma)\psi = 0, \tag{1}$$

where Σ corresponds to the retarded self-energy and embodies the background effects. For Dirac neutrinos, the chiral nature of neutrino interactions implies that, to one-loop order,

$$\Sigma = (a\not{k} + b\not{u})L, \tag{2}$$

where $L = (1-\gamma_5)/2$ and u^μ is the velocity four-vector of the medium; in its own rest frame $u^\mu = (1,\vec{0})$ and $k^\mu = (\mathscr{E},\vec{K})$. The coefficients a and b are complex functions of the scalars

$$\mathscr{E} = k\cdot u, \quad K = \sqrt{\mathscr{E}^2 - k^2}, \tag{3}$$

with $K = |\vec{K}|$. In the present context Σ corresponds to the Feynman diagram of Fig. 1, where the loop contains a relic (anti)neutrino from the thermal bath, with four-momentum $p^\mu = (E_p,\vec{p})$, and a Z boson with a blob indicating that we consider its decay width to all possible channels.

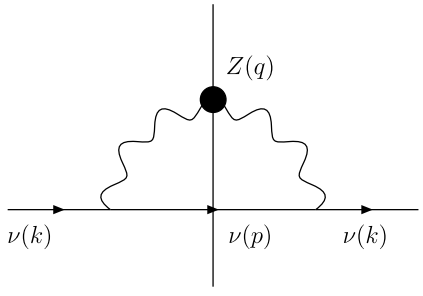

Fig. 1. Feynman diagram for the one-loop self-energy of an UHE neutrino due to a Z-boson exchange with an (anti-)neutrino from the relic background; the blob on the Z propagator indicates that we use the dressed propagator and the cut is to select the imaginary part of the diagram.

A consequence of the presence of a self-energy term in the equation of motion is to modify the dispersion relation of the incoming neutrino to

$$\mathscr{E}_K = \mathscr{E}_r - \mathrm{i}\frac{\gamma}{2}, \tag{4}$$

where $\mathscr{E}_K$, $\mathscr{E}_r$ and γ are functions of K. The real part, $\mathscr{E}_r$, is in general not equal to $\sqrt{K^2+m^2}$ but has some additional correction reflecting the dispersive interactions that can take place in the medium, while the imaginary part corresponds to the damping factor, or else said, to the total reaction rate [18]. For a constant damping, the survival probability of an UHE neutrino travelling through the relic neutrino background is

$$P_{\mathrm{T}}(\tau) = \mathrm{e}^{-\gamma\tau} \tag{5}$$

as a function of the propagation time τ.

The damping factor is directly related to the imaginary part of the self-energy Σ_i. In the real-time formalism of the FTFT, both the propagators and the self-energies become 2×2 matrices. As shown in [19], Σ_i can be expressed in terms of the off-diagonal elements of the self-energy matrix as

$$\Sigma_i = \frac{i}{2}(\Sigma_{12} - \Sigma_{21}). \tag{6}$$

The vertices of the theory are doubled compared to the vacuum case; the subscript 1 denotes the normal vertices of the Standard Model while the vertices labelled 2 get an extra minus sign. In our case, the expression for Σ_{12} as calculated from the Feynman diagram of Fig. 1 is

$$-\mathrm{i}\Sigma_{12} = \left(\frac{g}{2\cos\theta_{\mathrm{W}}}\right)^2 \int \frac{\mathrm{d}^4p}{(2\pi)^3}\mathrm{i}D_{21}^{\nu\mu}(q)\gamma_\mu L\mathrm{i}S_{12}(p)\gamma_\nu L, \tag{7}$$

with $D_{21}^{\mu\nu}(q)$ and $S_{12}(p)$ denoting the corresponding element of the Z boson and neutrino propagator, respectively. One obtains Σ_{21} by interchanging the indices 1 and 2 everywhere in Eq. (7).

Since the temperature of the medium is small compared to the boson mass, we may discard the thermal contribution to the Z propagator. Consequently, we have

$$D_{12}^{\mu\nu}(q) = 2\mathrm{i}\,\mathrm{Im}\,D^{\mu\nu}(q)\theta(-q\cdot u), \tag{8}$$

$$D_{21}^{\mu\nu}(q) = 2\mathrm{i}\,\mathrm{Im}\,D^{\mu\nu}(q)\theta(q\cdot u), \tag{9}$$

where θ is the step function and $D^{\mu\nu}(q)$ is the vacuum propagator for the Z boson. For $D^{\mu\nu}(q)$ we adopt the usual prescription around the resonance in the unitary norm [20–22]:

$$D^{\mu\nu}(q) = \frac{-g_{\mu\nu} + \dfrac{q_\mu q_\nu}{M^2}}{q^2 - M^2 + \mathrm{i}q^2\dfrac{\Gamma}{M}}. \tag{10}$$

Here M is the Z mass and Γ is the total width for Z decaying to fermion pairs. At lowest order Γ can be expressed, neglecting fermion masses, as:

$$\Gamma = \frac{\sqrt{2}G_F M^3}{6\pi}\sum_f N_f^c((I_f^3)^2 - 2I_f^3 Q_f \sin^2\theta_W + 2Q_f^2\sin^4\theta_W), \tag{11}$$

where G_F is the Fermi constant, $N_f^c = 1(3)$ for leptons (quarks), and I_f^3 and Q_f are the fermion isospin and charge, respectively [20]. The numerical values for Γ and M are taken from [23]. We assume that the Z boson decays in vacuum.

The propagators for the relic neutrino entering Eq. (7) are

$$S_{12}(p) = 2\pi i\delta(p^2 - m_\nu^2)[\eta_F - \theta(-p\cdot u)](\not{p} + m_\nu), \tag{12}$$

$$S_{21}(p) = 2\pi i\delta(p^2 - m_\nu^2)[\eta_F - \theta(p\cdot u)](\not{p} + m_\nu), \tag{13}$$

where

$$\eta_F = \theta(p\cdot u)f_\nu(P) + \theta(-p\cdot u)f_{\bar\nu}(P) \tag{14}$$

$$= \frac{\theta(p\cdot u)}{e^{\beta P-\alpha}+1} + \frac{\theta(-p\cdot u)}{e^{\beta P+\alpha}+1}, \tag{15}$$

with P denoting the magnitude of the three-momentum in the rest-frame of the background. The distribution of background relic (anti)neutrinos $f_\nu(P)$ ($f_{\bar\nu}(P)$) assumes a relativistic Fermi–Dirac form, with $\beta = 1/T_\nu$ and $\alpha = \mu/T_\nu$, μ being the chemical potential for neutrinos and T_ν the temperature of the relic neutrino bath. It is worth remarking here that, although relic neutrinos are not relativistic anymore at present time, their distribution maintains a relativistic form since their interactions froze out at their decoupling time, corresponding to $T_{\nu d}\sim 1$ MeV [24].

After replacing the expressions above in Eq. (6), expanding the delta function and neglecting contributions of order m_ν^2/M^2 coming from the term proportional to $q_\mu q_\nu$ in (10), one gets that

$$\Sigma_i = \left(\frac{g}{2\cos\theta_W}\right)^2 \int \frac{d^3P}{(2\pi)^3}\frac{\gamma_\mu \not{p}\gamma_\nu}{2E_p} L\{\mathrm{Im}[D^{\mu\nu}(p+k)]f_{\bar\nu}(P) + \mathrm{Im}[D^{\mu\nu}(p-k)][\theta(\mathscr{E}-E_p)(1-f_\nu(P)) + \theta(E_p-\mathscr{E})f_\nu(P)]\}, \tag{16}$$

where the integral is evaluated in the rest frame of the medium and we replaced p^0 by $E_p = (P^2+m_\nu^2)^{1/2}$ everywhere.

The first term corresponds to the resonant production of a Z boson through $\nu - \bar\nu$ annihilation; the factor of $f_{\bar\nu}(P)$ reflects the Pauli blocking acting on the antineutrinos in the background. The second and third terms correspond to the emission of a Z-boson respectively by the incoming neutrino ($\mathscr{E}_r > E_p$) or by the background antineutrino ($E_p > \mathscr{E}_r$). Both processes are kinematically forbidden and we drop them from this point on.

2.2. Ultra-relativistic approximation

Let us assume that the neutrino travelling through the relic neutrino thermal bath is ultra-relativistic and that we can neglect the background effects on its energy, i.e., $\mathscr{E}_r \simeq K$. In that case, we can use the following expression for the damping:

$$\gamma \simeq -2\,\mathrm{Im}\,b(K,K) = -\frac{1}{K}\mathrm{Tr}(\not{k}\Sigma_i)|_{\mathscr{E}_r=K}. \tag{17}$$

This expression was derived in [18] for the case of a massless fermion, but it can be shown that it remains valid for a massive one in the relativistic limit. The term proportional to $q_\alpha q_\beta$ in the Z propagator gives contributions of order m_ν^2/M^2; if we discard them, then the damping rate corresponding to the $\nu\bar\nu$ annihilation process reads

$$\gamma(K) = \frac{g^2}{\cos^2\theta_W}\frac{\Gamma}{M}\int\frac{d^3P}{(2\pi)^3}\frac{f_{\bar\nu}(P)}{2KE_p} \times \frac{(k+p)^2(k\cdot p)}{(1+\xi)(k+p)^4 - 2M^2(k+p)^2 + M^4},$$

where $\xi = \Gamma^2/M^2 \ll 1$ and $p^0 = E_p$. The previous formula can be conveniently rewritten in terms of the momentum integration of the cross-section for the process $\nu\bar\nu \to Z$, weighted by the corresponding statistical factor:

$$\gamma(K) = \int_0^\infty \frac{dP}{2\pi^2}P^2 f_{\bar\nu}(P)\sigma_{\nu\bar\nu}(P,K), \tag{18}$$

where

$$\sigma_{\nu\bar\nu}(P,K) = \frac{G_F}{\sqrt{2}}\frac{\Gamma M}{2K^2}\frac{1}{PE_P}\int_{s_-}^{s_+} ds\,\frac{s(s-2m_\nu^2)}{(s-M^2)^2+\xi s^2}. \tag{19}$$

Neglecting the chemical potential, the distribution function of the relic anti-neutrinos is:

$$f_{\bar\nu}(P) = f_\nu(P) = \frac{1}{e^{P/T_\nu}+1}. \tag{20}$$

The integration variable $s = (k+p)^2$ corresponds to the total energy in the center-of-mass and

$$s_\pm = 2m_\nu^2 + 2K(E_p \pm P). \tag{21}$$

The integral in Eq. (19) can be done in a closed form. For $m_\nu \ll M$, K, we get

$$\sigma_{\nu\bar\nu}(P,K) = \frac{2\sqrt{2}G_F\Gamma M}{2KE_p}\left\{\frac{1}{1+\xi} + \frac{M^2}{4KP(1+\xi)^2} \times \ln\left(\frac{(1+\xi)4K^2(E_p+P)^2 - 4M^2K(E_p+P) + M^4}{(1+\xi)4K^2(E_p-P)^2 - 4M^2K(E_p-P) + M^4}\right) + \frac{1-\xi}{(1+\xi)^2}\frac{M^3}{4KP\Gamma}\left[\arctan\left(\frac{2K(1+\xi)(E_p+P)-M^2}{\Gamma M}\right) - \arctan\left(\frac{2K(1+\xi)(E_p-P)-M^2}{\Gamma M}\right)\right]\right\}. \tag{22}$$

In Fig. 2, we plot the cross-section as a function of the UHEν energy K, for neutrino masses m_ν ranging from 10^{-1} eV to 10^{-4} eV. Each curve corresponds to a particular value of the relic neutrino momentum P. As expected, the thermal effects become more and more important as the ratio between the neutrino mass and the CνB temperature (which we take here as $T_{\nu 0}\simeq 1.69\times 10^{-4}$ eV) decreases. We also compare with the value of the cross-section in the

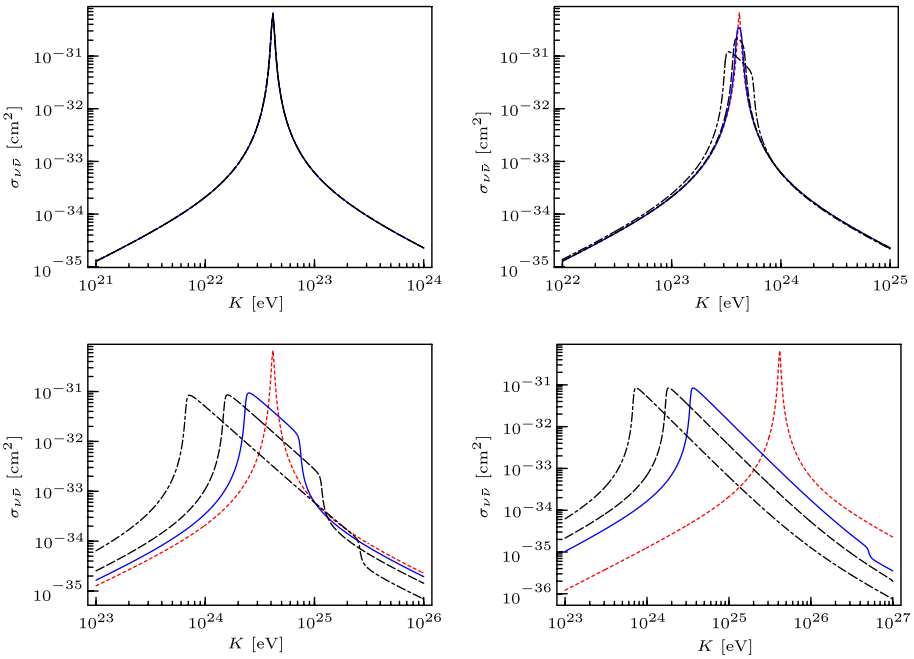

Fig. 2. Cross-section $\sigma_{\nu\bar{\nu}}(P,K)$, in cm^2, as given by Eq. (22), as a function of the energy of the incident neutrino, K and for neutrino masses of 10^{-1}, 10^{-2}, 10^{-3} and 10^{-4} eV (from left to right and top to bottom). Each plot shows four curves corresponding to different relic neutrino momenta; the dotted (red) curve correspond to the approximation of relic neutrinos at rest, $P=0$; the continuous (blue) curve is for $P_{\rm rms}=\sqrt{\langle P^2\rangle}\simeq 6.08\times10^{-4}$ eV and the dashed and dot-dashed (black) curves are respectively for $2P_{\rm rms}$ and $5P_{\rm rms}$. (For interpretation of the references in color in this figure legend, the reader is referred to the Web version of this article).

approximation of relic neutrinos at rest, $\sigma_{\nu\bar{\nu}}(0,K)$, which is obtained by taking the limit of $\sigma_{\nu\bar{\nu}}(P,K)$ for $P\to 0$. As long as the neutrino mass is sufficiently large, that is $m_\nu > 0.01$ eV, the cross-section does not vary significantly over the relevant range of P, i.e., the range of momenta selected by the CνB distribution function around the maximum of $P^2 f_\nu(P)$ at $P_{\rm max}\simeq 3.75\times10^{-4}$ eV. In this case, the position of the peak corresponds to the resonant energy $K^0_{\rm res}=M^2/2m_\nu$ for target neutrinos at rest. For smaller masses, the peak in the cross-section gets broader and shifts to smaller UHEν energies for increasing relic neutrino momentum. The maximum value is approximately constant over the relevant range of momenta, and is about one order of magnitude lower than $\sigma_{\nu\bar{\nu}}(0,K_{\rm res})$.

A simpler expression for $\sigma_{\nu\bar{\nu}}$ can be obtained using the mean value theorem by evaluating the integrand in Eq. (19) at the midpoint of the integration interval, $\bar{s}\simeq 2KE_p$. Taking into account that $s_+ - s_- = 4KP$ we get the following expression:

$$\bar{\sigma}_{\nu\bar{\nu}}(\bar{s}) = 2\sqrt{2}G_{\rm F}\Gamma M\frac{\bar{s}}{(\bar{s}-M^2)^2+\xi\bar{s}^2}, \tag{23}$$

where all the dependence on K and P is implicit in $\bar{s}=2K\sqrt{m^2+P^2}$.

We can use these expressions to evaluate the integral in Eq. (18) numerically. A common approximation consists in neglecting the thermal motion of the background neutrinos (see for example [6,16]). The corresponding expression can be recovered in our formalism by evaluating the cross-section (23) in $P=0$, i.e., in $\bar{s}_0=2m_\nu K$, or equivalently by taking the limit for $P\to 0$ of the general expression (22). The damping reads in this case:

$$\gamma^0(K) = \bar{\sigma}_{\nu\bar{\nu}}(\bar{s}_0)n_\nu \tag{24}$$

$$= 2\sqrt{2}G_{\rm F}\Gamma M\frac{2Km}{4(1+\xi)K^2m^2-4M^2Km+M^4}n_\nu, \tag{25}$$

with

$$n_\nu = n_{\bar{\nu}} = \int_0^\infty \frac{{\rm d}P}{2\pi^2}P^2 f_\nu(P). \tag{26}$$

Substituting the full expression for the total Z width to fermions, Eq. (11) into Eq. (25), one can easily recover the result of [6]. The expressions of [16] can be obtained by further evaluating the cross-section at the pole of the resonance $2mK_{\rm res}=M^2$ (narrow-width approximation).

The corresponding results are plotted in Fig. 3, where we directly compare the approximations for the damping factor, Eq. (25) and Eq. (23), with the exact expression obtained from Eqs. (18) and (22). The comparison is done for different values of the neutrino mass. One notices that the net effect of thermal broadening is a reduction of the damping, which affects the transmission probability and the depth and shape of the absorption dips.

Two effects combine: the modification of the cross-section peak due to its dependence on E_p, and the presence of the thermal distribution which selects a range of relic neutrino momenta comparable to the temperature of the CνB. Both effects contribute to smearing out the resonance peak and shifting its maximum value from $K_{\rm res}$ to lower energies. As long as the ratio m_ν/T_ν is $\gtrsim 100$, the position

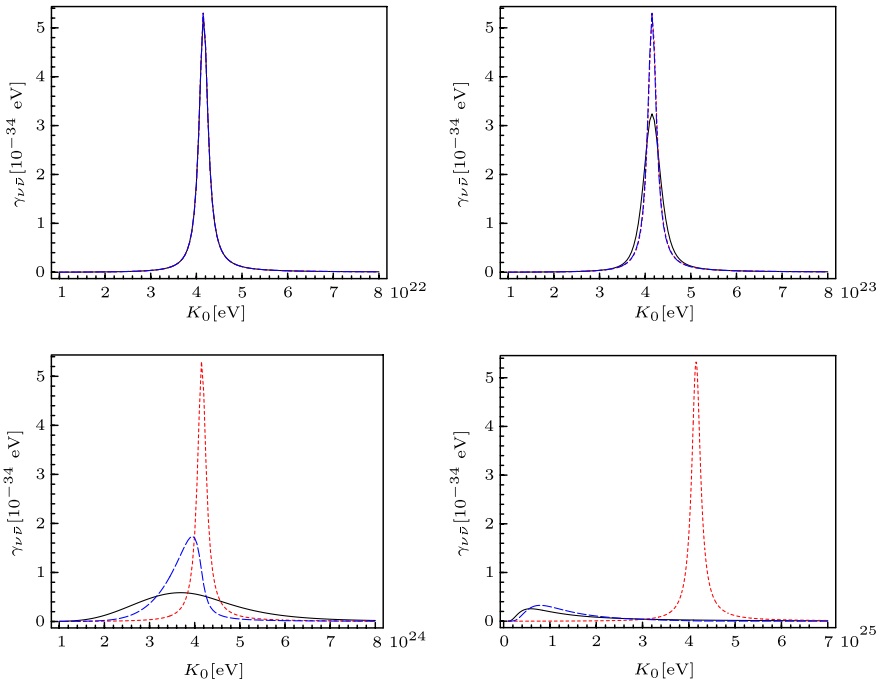

Fig. 3. Damping factor due to $\nu-\bar{\nu}$ annihilation, in eV, as a function of UHE neutrino energy K; each plot correspond to a given value of the neutrino mass (10^{-1} eV, 10^{-2} eV, 10^{-3} eV, 10^{-4} eV from left to right and from top to bottom) and displays the integrated damping, $\gamma_{\nu\bar{\nu}}$, from the full cross-section Eq. (22) (black, continued curve) and from the approximated cross-section Eq. (23) (blue, dashed curve), as well as the approximation for neutrinos at rest, $\gamma^0_{\nu\bar{\nu}}$, from Eq. (25) (red, dotted curve). The three curves are superposed for $m_\nu = 0.1$ eV, and so are the two approximations for $m_\nu = 0.01$ eV. (For interpretation of the references in color in this figure legend, the reader is referred to the Web version of this article).

of the peak is not significantly affected and the net effect is to reduce the damping. For smaller masses, the effect of thermal broadening is much stronger and the damping gets spread over a larger range of UHEν energies, resulting in a worse definition of the absorption dip.

The comparison of the exact and approximate results for the damping in Fig. 3 illustrates that none of the approximations is valid over the range of neutrino masses we consider. In the subsequent analysis we therefore keep on working with the full expression for the cross-section $\sigma_{\nu\bar{\nu}}(K,P)$, Eq. (22).

2.3. Transmission probability across the relic neutrino background

High energy neutrinos can travel cosmological distances almost without interacting. To calculate the damping by the CνB one has to take the expansion of the Universe into account. The standard procedure is to calculate the transmission probability by integrating the damping factor over the UHEν path, in terms of the redshift z, back to the source position z_s. The formula (5) is then generalised as follows:

$$P_T(K_0,z_s) = \exp\left[-\int_0^{z_s}\frac{dz}{H(z)(1+z)}\gamma_{\nu\bar{\nu}}(K_0(1+z))\right], \quad (27)$$

with the neutrino temperature $T_\nu = T_{\nu 0}(1+z)$. Both K_0 and $T_{\nu 0}$ refer to the quantities in today's Universe. For the Hubble factor we take $H(z) = H_0\sqrt{0.3(1+z)^3+0.7}$ as suggested by recent observations [25], with the numerical value of H_0 from [23].

Eq. (27) encompasses two effects due to the expansion of the Universe. First, the UHEν energy gets shifted, $K \to K_0(1+z)$. This broadens the absorption dip even in the approximation of relic neutrinos at rest, since the resonance energy changes along the UHEν path. Second, the temperature of the CνB gets shifted, $T_\nu \to T_{\nu 0}(1+z)$, i.e., the thermal bath of relic neutrinos is hotter at earlier times. This directly affects the ratio between m_ν and T_ν and results in a modification of the absorption properties of the CνB with respect to the UHEνs that cross it.

In Fig. 4 we show the transmission probability for an UHEν emitted at a fixed redshift $z_s = 1$, 5, 10 or 20, as a function of its present energy, K_0, and compare it with the results obtained in the approximation of relic neutrinos at rest.

As long as $m_\nu/T_\nu \gtrsim 10^2$, the shape of the absorption dip is not affected by thermal broadening and is rather sharply delimited, at high energies, by the bare resonant energy for the propagating neutrino, $K_{res} = M^2/(2m_\nu)$, and at low energies by the redshifted resonant energy $K_{res}/(1+z)$. Evaluating the position of these points would in principle allow us to determine the value of the neutrino mass as well as the redshift at which the UHEν was emitted. As m_ν/T_ν decreases, however, the absorption dips get shallower and broader, which complicates the extraction

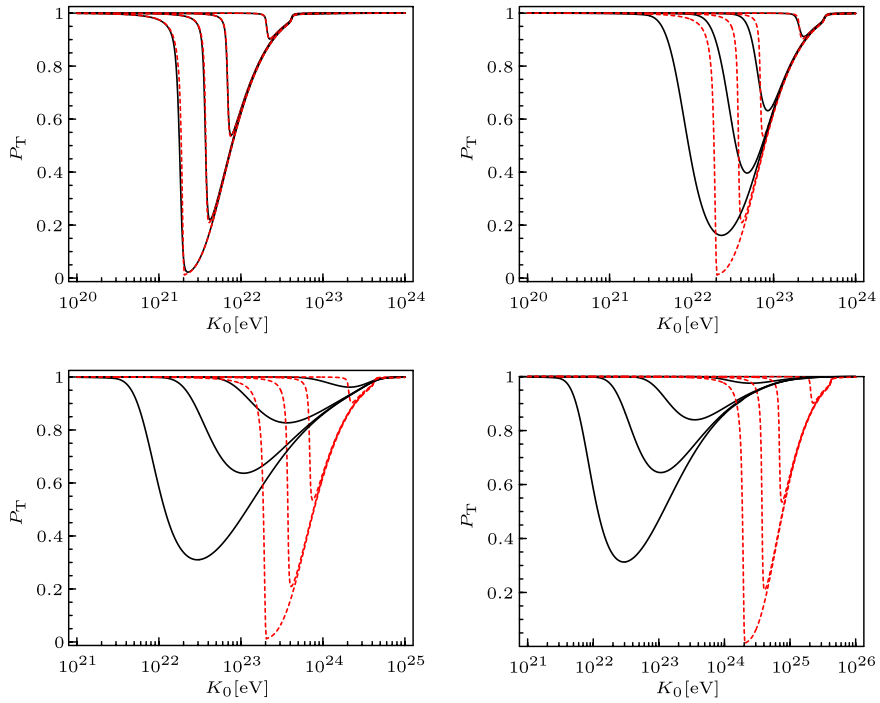

Fig. 4. Transmission probability $P_T(K_0, z_s)$ as a function of the incident neutrino energy as detected on Earth, K_0, for an UHE neutrino source located at redshifts $z_s = 1$, 5, 10, 20 (from top to bottom in each plot) and for a neutrino mass $m_\nu = 10^{-1}$, 10^{-2}, 10^{-3}, 10^{-4} eV. The continued, black curves corresponds to the full $\gamma_{\nu\bar{\nu}}$ from Eqs. (18) and (22), while the dotted (red) curves are for the approximation of relic neutrinos at rest, $\gamma^0_{\nu\bar{\nu}}$, from Eq. (25). (For interpretation of the references in color in this figure legend, the reader is referred to the Web version of this article).

of m_ν and z_s. The position of the minimum transmission probability is also shifted to lower energies. The effect of thermal motion increases with the redshift z since UHE neutrinos from more distant sources are emitted in hotter backgrounds.

3. Applications

The results presented so far deal with a monoenergetic source of UHE neutrinos located at a given redshift; let us now illustrate the potential effects of thermal motion on the process of absorption of UHE neutrinos in two more realistic contexts of physical relevance.

3.1. Absorption lines in a realistic UHE neutrino flux

The flux of UHE neutrinos at Earth depends on one hand on the mechanisms at work in the sources, which determine the injection spectrum of the UHE neutrinos, and on the other hand on the spatial and temporal distribution of the sources themselves. We follow here the approach of [16] and express the UHEν flux in function of the present neutrino energy K_0 as

$$\mathscr{F}_\nu(K_0) = \frac{1}{4\pi}\int_0^\infty \frac{dz}{H(z)} P_T(K_0, z)\mathscr{L}_\nu(K_0, z), \tag{28}$$

where $\mathscr{L}_\nu(K_0, z)$ is the neutrino source emissivity distribution, given in terms of the redshift z and the present energy of the UHEν. In the hypothesis of identical injection spectra for all sources, one can factorize the dependence in the redshift and write

$$\mathscr{L}_\nu(K_0, z) = \eta(z) J_\nu(K_0), \tag{29}$$

where $\eta(z)$ describes the distribution of the sources in the Universe, and $J_\nu(K_0)$ gives the number of neutrinos emitted per unit of energy by each of these sources. We use the following, standard ansatz [16,26,27]:

$$\eta(z) = \eta_0(1+z)^n \theta(z - z_{\min})\theta(z_{\max} - z); \tag{30}$$

$$J_\nu(K) = j_\nu K^{-\alpha}\theta(K_{\max} - K). \tag{31}$$

Eq. (30) is suitable for an approximate description of UHE neutrino sources distribution in models ranging from astrophysical acceleration sites ("bottom-up" mechanisms, for which we can take $n \simeq 4$ and $z_{\max} \leqslant 10$) to exotic, non-accelerator sources (which have $n \simeq 1$ to 2 and may extend to a much larger $z_{\max}$). In both cases, we take the lower bound for the source distribution to be $z_{\min} = 0$. The spectral index α typically ranges between 1 and 2, depending on the production mechanism considered; we assume here that it is constant over the range of energies examined and do not consider the possibility of broken power-law spectra above the GZK energy. We also suppose that $K_{\max} > K_{\rm res}(1+z)$ in all our analysis.

Under these assumptions, as pointed out in [16], the only dependence on the spectral indexes α and n enters through a difference $n - \alpha$. We consider here, for the purpose of illustrating our results, two distinct situations: $n - \alpha = 2$ which could describe the UHE neutrino flux

expected from an astrophysical, bottom-up-type source, and $n - \alpha = 0$ which would rather be associated to UHE neutrino fluxes produced in top-down processes. Results are presented in Fig. 5, which displays the UHEν flux, Eq. (28), as a function of the present energy K_0 of the UHEν, after normalization to the flux in the absence of absorption effects, $\mathscr{F}_{\nu 0}$ (obtained by replacing $P_T(K_0, z) = 1$ in Eq. (28)). The first column corresponds to $n - \alpha = 2$ and for each value of m_ν we show several curves corresponding to different redshift limits for the source population, $z_{max} = 2, 5, 10$, while the second column corresponds to $n - \alpha = 0$ and redshift limits $z_{max} = 10, 20$.

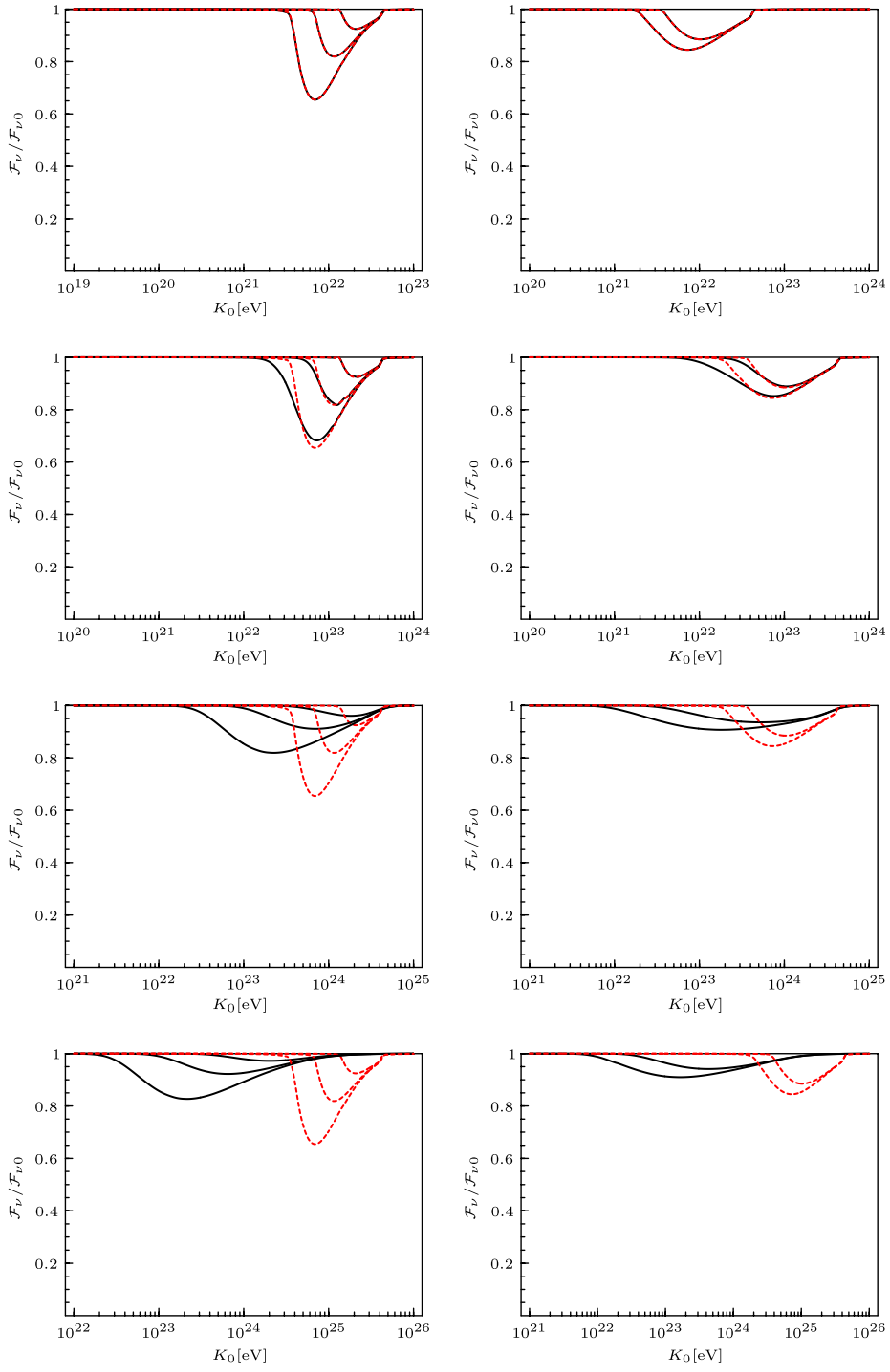

Fig. 5. UHE neutrinos fluxes in presence of damping, $\mathscr{F}_\nu$, normalized to the corresponding flux in absence of interactions, $\mathscr{F}_{\nu 0}$, for a neutrino mass $m_\nu = 10^{-1}, 10^{-2}, 10^{-3}, 10^{-4}$ eV (from top to bottom). The black (continued) curves are for the exact expression using Eq. (22) while the dotted, red curves are for the approximation of neutrinos at rest, Eq. (25). The left column is for $n - \alpha = 2$ and $z_{max} = 2, 5, 10$ (from top to bottom in each plot), while the right column is for $n - \alpha = 0$ and $z_{max} = 10, 20$. (For interpretation of the references in color in this figure legend, the reader is referred to the Web version of this article).

In that range of parameters, one can see that thermal effects do not significantly affect the shape of the absorption dip in the UHE neutrino flux as long as $m_\nu/T_\nu \gtrsim 10^2$. In particular, the endpoint of the dip at high energies, corresponding to $K_{\rm res}$, is well-defined and can be used to estimate the absolute value of m_ν, provided the absorption dip is not too shallow nor too narrow to be resolved experimentally. The global shape of the dip clearly depends on the value of $n-\alpha$. Assuming that the spectral index α can be determined from the measurements of the UHEν spectrum in the range of energies which is not affected by the absorption, one could then obtain information on n and therefore on the development of the source population. From the endpoint of the absorption dip at low energies, which corresponds to the resonance energy of the neutrinos emitted at the largest redshift, $K_0(1+z_{\rm max})$, one can also estimate the epoch at which the UHEν sources appeared.

For smaller values of the ratio m_ν/T_ν, the situation is significantly complicated by the thermal motion of relic neutrinos. As a result of the broadening of the transmission probability, the dips get shallower and can extend over several orders of magnitude in energy, depending on the maximum redshift chosen for the source distribution. This might complicate their observation, especially at small redshifts. From the figure one sees indeed that for $z_{\rm max} \leqslant 2$, the flux would not be depleted more than a 5%. Results will also be more difficult to interpret in terms of a prediction for the neutrino mass and the maximum redshift for the population of sources, since the position of the end points of the absorption dip is not so clearly defined anymore. On the other hand, maximum absorption is now achieved at lower energies K_0. The shift is significant, even more than an order of magnitude for very small masses, $m_\nu \approx 10^{-4}$ eV. In view of the inverse-power-law form of the UHEν energy spectrum, this could significantly help to improve the detection potential, even though the energy range $10^{23}-10^{24}$ eV, is currently beyond the reach of the majority of UHEν experiments planned (see for example [16]).

3.2. Absorption lines due to relic neutrino clustering

The possibility that massive relic neutrinos cluster onto dark matter halos has been intensively studied, in particular in relation with the generation of the UHE cosmic rays through the Z-burst mechanism [10,9,11]. Recent works have presented revised estimations of the density profiles and typical spatial extension of the neutrino clusters [28,29], giving overdensities of the order of 10–10^4 with respect to the present background density. They can extend on scales $L \sim 0.01$–1 Mpc, depending on the neutrino mass, the mass of the attracting halo, and its velocity dispersion (which is typically of the order of 200 km/s for a galaxy and 1000 km/s for a galaxy cluster). This last parameter also constrains the epoch at which clustering can start, since neutrinos cannot be efficiently trapped as long as their mean velocity,

$$\langle v_\nu \rangle \simeq 1.6\times 10^2(1+z)\left(\frac{\rm eV}{\rm m}\right)\ {\rm km\ s^{-1}}, \tag{32}$$

is larger than the velocity dispersion of the attracting galaxy or galaxy cluster [29]. For neutrinos with masses $\lesssim 1$ eV, clustering will thus take place at very small redshifts and we can safely ignore the effect of the expansion of the Universe in this analysis. Other important limiting factors to the clustering of neutrinos on large scales are Pauli blocking and the limit on the maximum phase-space density, as described in [30]. They actually imply that only neutrinos with mass $m_\nu \gtrsim 1$ eV will efficiently cluster on galactic halos, on typical scales $L_{\rm G} \sim 50$ kpc, while neutrinos with mass $m_\nu \gtrsim 0.1$ eV can cluster on scales as big as $L_{\rm C} \sim 1$ Mpc in halos associated to (super-)clusters of galaxies [10,28,29].

The effect of neutrino clustering is limited to small scales and the overdensities are not large enough to have a significant incidence on the damping of UHEν travelling on cosmological distances, except maybe in the case of galaxy superclusters like Virgo [31].

To compute the absorption by clustered neutrinos, one has to substitute a suitable distribution function $f^{\rm cl}(P)$ inside the cluster into Eq. (18). To make a simple estimation of the effect, we assume that $f^{\rm cl}(P)$ does not depend on the position, i.e., we take a constant neutrino overdensity. Outside of the cluster, the neutrino density is that of the CνB. For $f^{\rm cl}(P)$, we make the ansatz of a modified Fermi–Dirac distribution

$$f^{\rm cl}(P) = \frac{1}{2}\frac{{\rm e}^{-\Phi/T_\nu}+1}{{\rm e}^{(P-\Phi)/T_\nu}+1}. \tag{33}$$

This distribution parametrises reasonably well the distribution functions presented by [29] in terms of a single parameter Φ, keeping the temperature T_ν unchanged from the CνB. The neutrino density which corresponds to Eq. (33) is

$$n_\nu^{\rm cl} = -\frac{T_\nu^3}{2\pi^2}(1+{\rm e}^{-\Phi/T_\nu}){\rm Li}_3(-{\rm e}^{\Phi/T_\nu}), \tag{34}$$

where ${\rm Li}_3(x)$ is the trilogarithm function. For a given overdensity factor $N^{\rm cl}$ we solve $n_\nu^{\rm cl} = N^{\rm cl} n_{\nu 0}$ numerically for Φ.

The clusters we consider in the following have an overdensity factor $N^{\rm cl}$ between 10 and 10^4 according to the results mentioned earlier, and a spatial extension $L_\nu^{\rm cl}$. We study the case where the cluster is located between the source of the UHEν and the observer and compute the transmission probability for neutrino masses of 1 eV and 0.1 eV.

As expected, the effect of the thermal motion of the relic neutrinos is in general negligible or small due to the relatively small overdensities achievable. We have to saturate the bounds on the parameters to get a significant effect, as shown in Fig. 6, which displays the transmission probability with and without thermal effects, for a cluster of relic neutrinos with mass $m_\nu = 0.1$ eV and extension 1 Mpc. For a maximal overdensity factor $N^{\rm cl} = 10^4$ the thermal motion reduces the maximum absorption probability across the cluster from ≈55% to ≈35%, contributing to reducing its

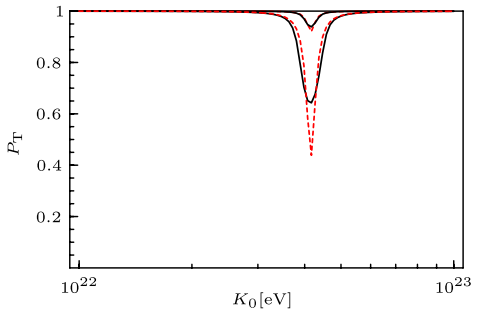

Fig. 6. Transmission probability for a cluster of extension 1 Mpc, made of neutrinos of mass 0.1 eV, with a constant neutrino density $n_\nu^{cl} = 10^3 n_{0\nu}$ and $n_\nu^{cl} = 10^4 n_{0\nu}$. The color code is the same as in previous figures. (For interpretation of the references in color in this figure legend, the reader is referred to the Web version of this article).

effect respect to the non-clustered CνB absorption probability shown in Fig. 4.

4. Conclusions

Using the formalism of finite-temperature field theory we have calculated the damping factor of an UHEν propagating through the CνB including the effects of the thermal motion of the relic neutrinos in a systematic way. This allowed us to generalise the expressions for the transmission probability P_T that are commonly used in the literature.

From the exploration of the parameter space allowed by cosmological and astrophysical constraints as well as by current limits on the neutrino mass, we see that thermal effects significantly affect the shape and position of the absorption dips in a realistic UHEν flux as soon as the ratio between the neutrino mass and the CνB temperature goes below $\approx 10^2$, i.e., well before the relic neutrinos become relativistic. As expected, the effect essentially consists in smearing out the dip and shifting its minimum value to lower energies. This will complicate the observation of the dip in a real experiment measuring neutrino fluxes, especially if the UHEν source population is concentrated at small redshifts, producing rather shallow and extended dips. The shift of the absorption dip to lower energies, where neutrino fluxes are expected to be higher, increases in principle the potential of detection of the effect respect to the case of a neutrino at rest with the same mass. Still, the situation could become more intricate if the pattern of neutrino mass eigenstates is such that their combined effect results in a superposition of dips with different depths and extensions.

In the context of neutrino mass spectroscopy, we see from the examples that thermal effects do not affect the determination of the endpoint of the absorption dip, and hence the possibility of extracting information on the absolute neutrino mass, as long as $m_\nu \gtrsim 0.01$ eV, which is verified by at least one neutrino in the currently favoured mass schemes [32]. As the absorption dips get broader and shallower, the prospects for determining efficiently the resonance energy get worse as the endpoint of the absorption dip is no longer sharply defined.

Finally, as another application of our formalism, we have also investigated the transmission probability for UHE neutrinos propagating through a relic neutrino cluster. In the standard context of neutrino clustering around galaxies or galaxy clusters, we found that the thermal motion can further reduce the absorption effect of the cluster. This absorption is small compared to the absorption of UHEν in the CνB for neutrinos travelling cosmological distances, since clustering only occurs at small redshifts.

Acknowledgements

We would like to acknowledge support by CONACyT under grants 34868-E and 46999-F and by DGAPA-UNAM under grants PAPIIT IN116503, IN119405 and IN112105.

References

[1] P.J.E. Peebles, Principles of Physical Cosmology, Princeton University Press, 1993.
[2] E.W. Kolb, M.S. Turner, The Early Universe, Addison-Wesley, Redwood City, 1990.
[3] T.J. Weiler, Phys. Rev. Lett. 49 (1982) 234.
[4] T.J. Weiler, Astrophys. J. 285 (1984) 495.
[5] P. Gondolo, G. Gelmini, S. Sarkar, Nucl. Phys. B 392 (1993) 111. Available from: <arXiv:hep-ph/9209236>.
[6] E. Roulet, Phys. Rev. D 47 (1993) 5247.
[7] S. Yoshida, Astropart. Phys. 2 (1994) 187.
[8] S. Yoshida, H.y. Dai, C.C.H. Jui, P. Sommers, Astrophys. J. 479 (1997) 547. Available from: <arXiv:astro-ph/9608186>.
[9] D. Fargion, B. Mele, A. Salis, Astrophys. J. 517 (1999) 725. Available from: <arXiv:astro-ph/9710029>.
[10] T.J. Weiler, Astropart. Phys. 11 (1999) 303. Available from: <arXiv:hep-ph/9710431>.
[11] E. Waxman. <arXiv:astro-ph/9804023>.
[12] S. Yoshida, G. Sigl, S.J. Lee, Phys. Rev. Lett. 81 (1998) 5505. Available from: <arXiv:hep-ph/9808324>.
[13] J.J. Blanco-Pillado, R.A. Vazquez, E. Zas, Phys. Rev. D 61 (2000) 123003. Available from: <arXiv:astro-ph/9902266>.
[14] H. Pas, T.J. Weiler, Phys. Rev. D 63 (2001) 113015. Available from: <arXiv:hep-ph/0101091>.
[15] D. Fargion, M. Grossi, P.G. De Sanctis Lucentini, C. Di Troia, R.V. Konoplich, in: H.V. Klapdor-Kleingrothaus (Ed.), Dark Matter in Astro and Particle Physics, Dark 2000, Heidelberg, 10–14 July, Springer, 2001, p. 455. Available from: arXiv:astro-ph/0102426; D. Fargion, P.G. De Sanctis Lucentini, M. Grossi, M. De Santis, B. Mele, Mem. Soc. Ast. It. 73 (2002) 848. Available from: <arXiv:hep-ph/0112014>.
[16] B. Eberle, A. Ringwald, L. Song, T.J. Weiler, Phys. Rev. D 70 (2004) 023007. Available from: <arXiv:hep-ph/0401203>.
[17] G. Barenboim, O. Mena Requejo, C. Quigg, Phys. Rev. D 71 (2005) 083002. Available from: <arXiv:hep-ph/0412122>.
[18] J.C. D'Olivo, J.F. Nieves, Phys. Rev. D 52 (1995) 2987. Available from: <arXiv:hep-ph/9309225>.
[19] J.C. D'Olivo, J.F. Nieves, Phys. Lett. B 359 (1995) 148. Available from: <arXiv:hep-ph/9508394>.
[20] F. Berends et al., The Z line shape, in: G. Altarelli, R. Kleiss, C. Verzegnassi (Eds.), CERN Yellow Report 89-08, vol. 1, 1989, p. 89.
[21] D.Y. Bardin, A. Leike, T. Riemann, M. Sachwitz, Phys. Lett. B 206 (1988) 539.
[22] A. Borrelli, M. Consoli, L. Maiani, R. Sisto, Nucl. Phys. B 333 (1990) 357.
[23] S. Eidelman et al., Phys. Lett. B 592 (2004) 1.

[24] P. Langacker, J.P. Leveille, J. Sheiman, Phys. Rev. D 27 (1983) 1228.
[25] D.N. Spergel et al. [WMAP Collaboration], Astrophys. J. Suppl. 148 (2003) 175. Available from: <arXiv:astro-ph/0302209>.
[26] O.E. Kalashev, V.A. Kuzmin, D.V. Semikoz, G. Sigl, Phys. Rev. D 66 (2002) 063004. Available from: <arXiv:hep-ph/0205050>.
[27] D.V. Semikoz, G. Sigl, JCAP 0404 (2004) 003. Available from: <arXiv:hep-ph/0309328>.
[28] S. Singh, C.P. Ma, Phys. Rev. D 67 (2003) 023506. Available from: <arXiv:astro-ph/0208419>.
[29] A. Ringwald, Y.Y.Y. Wong, JCAP 0412 (2004) 005. Available from: <arXiv:hep-ph/0408241>.
[30] S. Tremaine, J.E. Gunn, Phys. Rev. Lett. 42 (1979) 407.
[31] A. Ringwald, T.J. Weiler, Y.Y.Y. Wong. <arXiv:astro-ph/0505563>.
[32] J.F. Beacom, N.F. Bell, Phys. Rev. D 65 (2002) 113009. Available from: <arXiv:hep-ph/0204111>.